Asphalt mixture performance and testing

# Viscoplastic modelling of asphalt concretes: application to innovative ballastless railway structural design

*Octavio Lopez-Polanco[1], Talita Alves[2], Thomas Gabet[2], Nicolas Calon[1], Pierre Hornych[2]*
*[1]SNCF réseau, [2]IFSTTAR - materials and structures dpt.*

Abstract

An original concept of railways was assessed. A classical railway track is made of rails supported by sleepers and ballast. The innovative track studied here is made of rails continuously supported by an asphalt concrete layer. Neither sleepers nor ballast are used in such a structure. This concept was developed to limit the thickness of railway structures in tunnel and increase their gauge, while reducing spending for tunnel rehabilitation. This railway concept was developed inside a French project named 'REVES', funded by the French government. It aims at developing a technical solution from the pre-design to an on-site demonstrator. It should validate the railway structure concept for commercial use on the French national network. As a part of this project, a PhD thesis was funded by SNCF-Réseau and scientifically led by IFSTTAR. It aimed at studying on the behaviour of the asphalt concrete layer under peculiar loadings related to railway freight. The viscoplastic behaviour of asphalt concretes under heavy and concentrated loads was the focal point of the PhD thesis. Despite the behaviour of asphalt concretes in roads under truck traffic being relatively well understood, freight trains can lead to double the usual truck loads and concentrate these loads under the rails. A viscoplastic model was developed, based on the Perzyna model of standardized viscoplasticity, using a Drucker-Prager criterion closed by a cap. This model was set up and assessed by means of a first experimental program of triaxial tests on highly deformable asphalt concretes. A second experimental program was performed on the high performance asphalt concrete that would be used in railway infrastructures. The parameters of the viscoplastic model were identified. They validated the model used and allowed to perform some predictions of the long term behaviour of such an asphalt concrete structure related to settlement and permanent deformation.

This paper was first published in 2020 in version 1.0 of the proceedings of the 7th E&E Congress. This second edition (version 1.1.) of the proceedings is published in June 2021. The content of this paper has not changed, but the author(s) may have provided additional information in the form of an annex.

## 4. INTRODUCTION

This paper presents the experimental and numerical results of a research on the resistance of an asphalt concrete (AC) loaded by rails on a continuous support for railway applications. This research is part of a project named REVES, which aims to reduce the thickness of railway infrastructures profile inside tunnels, in a way to maximize its gauge. The use of AC is not so usual for manufacturing railway tracks. It is mainly found as an alternative subballast material [1,2]. Some tracks in the world are also built on an AC layer, without using any ballast, as the concepts of GETRAC, ATD and SATO [3]. On those cases, rails are laid on sleepers directly supported on the asphalt concrete. The innovative concept proposed here is slightly different. It aims at decreasing the thickness of the railway track by laying the rails continuously on the AC, without using neither ballast nor sleepers. Such a structure without ballast was already used in the Chamartin tunnel, in Spain, but the rails were embedded in a cement concrete layer and not an asphalt concrete layer.

Using an AC to replace old railway infrastructures on tunnel sections may have some interesting impacts on the structural and functional performance of the track. Indeed, such infrastructure is thinner than a standard granular one, which also leads to environmental and constructive advantages [4]. Being faster to manufacture due to the use of AC, it allows the fast opening to circulation of vehicles and equipment on the platform during the construction phase.

Such an innovative structure may present different types of damage: fatigue cracking and rutting due to repeated loadings coming from the traffic of trains, and settlement due to a train stopping on the track. This last damage is typically due to the viscoplastic behaviour of AC. The typical case of a train stopping in the tunnel is assessed here, as the worst-case configuration. The work presented deals with the specific problem of rail settlement due to permanent strains in the AC. It does not present the fatigue resistance design, correlated to the freight traffic. Therefore, no dynamic effect is taken into account.

An experimental program of triaxial creep tests was carried out on a high performance AC in order to characterize the triaxial behaviour of this viscoplastic and granular material. Based on this experimental campaign, parameters of a viscoplastic model based on the Perzyna formulation were identified. Then, structural simulations were performed using a FEM code, allowing a better understanding of the evolution of stress fields under static loading, and showing that strains and settlements of such structure seem to be acceptable according to the French Railway standards.

## 5. EXPERIMENTAL PROGRAM

### 5.1. Material

**The Material: a base course bituminous mix of GB4 type**
The tested material is a GB4 (grave-bitumen), a high performance hot mix asphalt designed in accordance with the French standards. The maximum grain size is 14 mm and the bitumen used is of 35/50 grade. The air voids content for the tested GB4 mixture is 4%. The grading curve is given in Table 1.

Table 1. Aggregate size distribution.

| Diameter of particle (mm) | % Passing obtained | % Passing theoretical |
|---|---|---|
| 16 | 98.5 | 100 |
| 14 | 95.5 | 96 |
| 12.5 | 89.4 | 90 |
| 10 | 76.5 | 77 |
| 8 | 64.8 | 66 |
| 6.3 | 53.9 | 56 |
| 4 | 40.3 | 44 |
| 2 | 28.5 | 32 |
| 1 | 19.4 | 24 |
| 0.5 | 13.3 | 18 |
| 0.25 | 9.5 | 14 |
| 0.125 | 7.1 | 10 |
| 0.063 | 5.9 | 6.5 |

A complex modulus test was performed according to the standard EN 12697-26 [5]. The complex modulus of the material (15300 MPa) was assessed at 15°C and 10 Hz. A fatigue test was also performed according to the standard EN 12697-24 [6], leading to a fatigue strain value of $\varepsilon_6$=132µdef at 10°C and 25 Hz.

**Sample preparation**
Samples were compacted using a gyratory compactor at hot temperature, then cored and sawed to obtain Ø 80mm x 160mm cylindrical specimens (Figure 1). This preparation method makes it possible to eliminate all boundary effects due to the mould and to obtain a very homogeneous material.

Figure 1. Coring of a sample obtained from a gyratory compactor press, followed by its sawing to reach the dimensions of Ø80x160 mm.

### 5.2. Triaxial testing device

The principle of a triaxial test consists in applying an axial load leading to a deviator stress q, and a confining pressure $\sigma_{rad}$ by means of a triaxial cell. The experimental device used for this test has been widely used for characterizing AC [7,8]. The Schenk hydraulic press depicted in Figure 2 has a loading capacity of 100kN and a strokr of 100 mm. The triaxial cell can apply a pressure of 700 kPa. Axial and radial strains are measured using LVDT sensors attached to the central part of the sample. Two vertical sensors and one radial sensor allow the determination of axial and radial strains on the sample during the load cycles.


**(a)** **(b)** **(c)**

Figure 2. (a) Triaxial test principle, (b) hydraulic press and (c) instrumented sample, with two axial LVDTs (1 visible on the picture) and a ring with an LVDT for measuring radial strains.

### 5.3. Testing program

29 triaxial tests were performed covering a range of deviator stresses from 400 to 1000 kPa, and confining pressures of 0 to 500 kPa, as depicted in Table 2. Some tests were performed in order to evaluate the repeatability of the procedure. They showed a noticeable discrepancy, reaching 30% for confined tests. These results and more comments on the possible causes of such scatter are available on [9], but are not presented here.

Table 2. Triaxial tests loading combinations.

| Test | q (kPa) | σrad (kPa) | Air voids (%) |
|---|---|---|---|
| 1 | 400 | 0 | 5.4 |
| 2 | 400 | 50 | 5.3 |
| 3 | 400 | 100 | 5.4 |
| 5 | 800 | 200 | 4.6 |
| 6 | 400 | 25 | 5.2 |
| 9 | 1500 | 400 | 4.4 |
| 10 | 1500 | 200 | 4.3 |
| 11 | 1200 | 500 | 5.2 |
| 12 | 1200 | 200 | 4.7 |
| 13 | 1200 | 100 | 4.7 |
| 14 | 1000 | 200 | 4.3 |

| Test | q (kPa) | σrad (kPa) | Air voids (%) |
|---|---|---|---|
| 15 | 1000 | 500 | 4.8 |
| 16 | 800 | 500 | 4.7 |
| 17 | 800 | 0 | 4.5 |
| 18 | 600 | 0 | 4.5 |
| 19 | 1000 | 500 | 5.5 |
| 20 | 800 | 0 | 4.5 |
| 21 | 800 | 100 | 3.7 |
| 27 | 1000 | 200 | 4.4 |
| 28 | 800 | 200 | 4.4 |
| 29 | 800 | 200 | 3.9 |

## 6. EXPERIMENTAL RESULTS

### 6.1. Effect of the confining pressure. Series at q = 800kPa

The results presented in this section concern tests are those performed with the deviator "q" maintained at 800kPa, covering the four levels of confining pressure $\sigma_{rad}$ (0, 100, 200 and 500 kPa). On Figure 3, axial and radial strains are plotted as function of time. In accordance with the soil mechanics' convention, compression strains are positive.

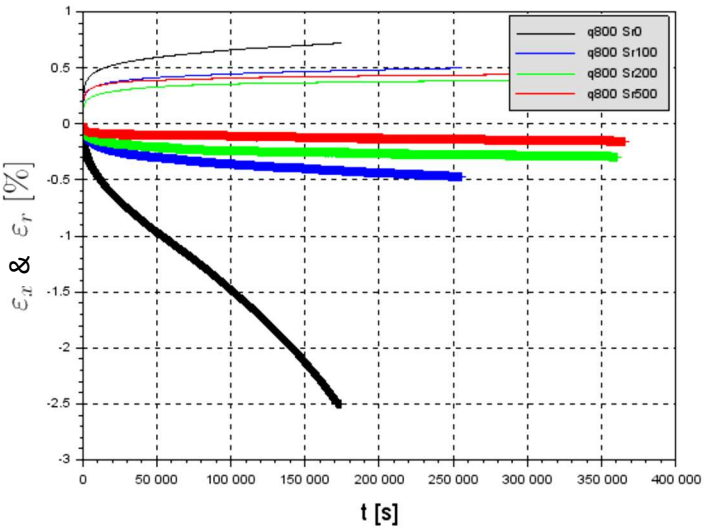


Figure 3. Axial and radial strains for q = 800 kPa and $\sigma_{rad}$ = 0, 100, 200 and 500 kPa.

It can be noticed from Figure 3 that the confining pressure has a strong influence on the strain response of the GB4. The unconfined sample (curve in black) presents higher strain magnitudes than the other samples, and its curve in function of time presents higher slope. At 100 000 seconds a tertiary creep with an increase of the slope is noticed for the unconfined sample. For the confined samples, the strains tend to stabilize in the long term, with no viscoplastic flow. The radial strains, negative, under zero, tend to show a ranking in accordance with the level of confinement. The axial strains, positive, mostly respect this same ranking, except for the confining pressure of 200 and 500 kPa. The results are in good accordance with previous studies [7]. They highlight the importance of using a generalized viscoplastic law to model such creep tests and permanent strain phenomena appearing in asphalt concrete under static loadings.

Figure 4 presents the volumetric strains, plotted as function of time for the four levels of confinement. It should be noted that in the soil mechanics convention used in this study a positive bulk strain corresponds to a contractant behaviour of the material. Only the highest confining pressure (500 kPa) leads to a contractant volumetric behaviour (curve in red). The three other samples indicate an immediately dilatant response. The less the sample is confined, the faster the volumetric dilation appears. The unconfined material presents significantly higher volumetric strains than the confined samples (curve in black). This result highlights the importance of taking into account the triaxial state of stress when analysing the material's strain response.

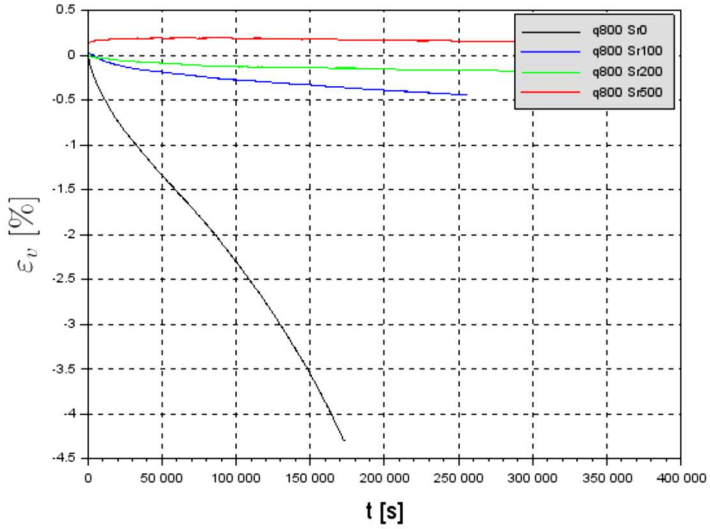


Figure 4. Volumetric strains for q = 800 kPa and $\sigma_{rad}$ = 0, 100, 200 and 500 kPa.

### 6.2. Effect of the deviator stress. Series at $\sigma_{rad}$ = 200 kPa

The results presented in this section concern tests performed with the confining pressure ($\sigma_{rad}$) maintained at 200kPa, considering the four levels of axial deviator stress "q" (800, 1000, 1200 and 1500 kPa). On Figure 5, axial and radial strains are plotted as function of time for the four levels of deviator stress. In accordance with the soil mechanics' convention, compression strains are positive.

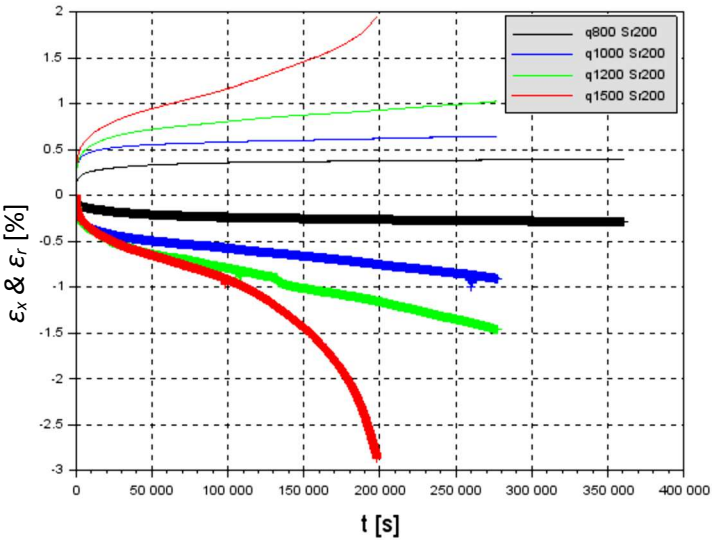


Figure 5. Axial and radial strains for $\sigma_{rad}$ =200 kPa and q=800, 1000, 1200 and 1500 kPa.

At the same confining pressure, a strong influence of the deviator stress can be observed on the answer of the GB4 in terms of strains. At high values of deviator stress (curve in red), the AC sample showed a very fast and more important decrease in terms of strains than at low values of deviator stress. For the red curve on Figure 5, at 100 000 seconds, a tertiary creep with a fast increase of the slope can be observed, which does not happen with the other curves. The low deviator stress sample (curve in black) tend toward a horizontal plateau, corresponding to a stabilization of the strains with no viscoplastic flow. The radial strains, as the axial strains, tend to show a rank in accordance to the level of deviator stress. This series of tests also shows the need of taking into account both deviator stress and confinement to understand the TRX behaviour of asphalt concretes.

## 7. MODELLING VISCOPLASTICITY

### 7.1. Perzyna's viscoplastic model

The objective of this work was to develop a model as simple as possible, while considering the effect of confinement and the contractant/dilatant behaviour of the GB4. It led to build a standard associated viscoplastic model that requires the determination of only five parameters.
The Perzyna flow rule is used for the model. With this rule, the viscoplastic strain rate $\dot{\varepsilon}^{vp}$ is defined by:

$$\underline{\underline{\dot{\varepsilon}}}^{vp} = \frac{1}{\eta}\langle f \rangle^N \frac{\partial f}{\partial \underline{\underline{\sigma}}},$$

With f being the yield surface, $\langle f \rangle$ the positive part of the yield function f, and *f1* and *f2* determined as follow:

$$f_1 = cos(\alpha)\, q - sin(\alpha)\, q$$
$$f_2 = \sqrt{(p - p_c)^2 + q^2} - p_c sin(\alpha)$$
$$p_c = p_{c0}\,(1 + b\,\varepsilon_d)$$

The two functions f1 and f2 correspond graphically to the slope and to the circle on the scheme depicted in Figure 6, respectively. $\eta$ is a viscosity parameter and $N$ is an exponent determined experimentally. The chosen yield function is a Drucker-Prager cone closed by a spherical cap. In the stress invariants space (p,q), the yield function is a slope closed by a circle (Figure 6). The Drucker-Prager slope represents the behaviour of the granular skeleton of the asphalt concrete. The cap function allows the GB4 to model both dilatant and contractant behaviours. The hardening variable is "$p_c$", the position of the centre of the circular cap on the p axis, while "b" is the hardening parameter. The latter regulates the evolution of the circular part of the yield surface along the Drucker-Prager slope (Figure 6).

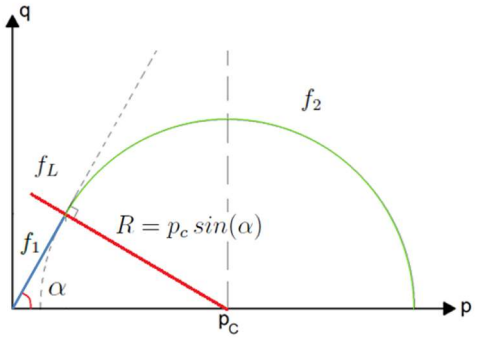


Figure 6. Yield surface of the Perzyna model. A Drucker-Prager line (in blue) closed by a circular cap model (in green).

### 7.2. Parameters identification

A parameters' identification method was developed to identify the set of five parameters. As they are mostly independent from each other, they can be fitted sequentially. The identification process follows this order:

- N: the power of the function initially set to 3.
- $p_{c0}$: the position of the center of the circle on the p axis. This parameter determines, for a given stress state, the material initial dilatancy or contractancy. For a given (p,q) stress state, if $p_{c0} > p$, the material initially dilates. If $p_{c0} \leq p$, the material is initially contractant. This parameter is fitted by means of triaxial creep tests presenting no initial volumetric strain.
- $a = tan(\alpha)$: the Drucker-Prager slope separates tests that stabilize over time from unstable tests. On the (p,q) graph, unstable stress states are located to the left side of the slope.
- $b$: the hardening parameter, which determines the final strain levels for stabilizing tests. It is identified by examining the final states of a series of stabilized triaxial tests.
- $\eta$: the viscosity parameter is fitted in order to adjust the kinetics of the strain curves.

The set of parameters obtained while fixing N=3 is presented in Table 3.

Table 3. Set of parameters

| $a$ | $p_{c0}$ (MPa) | $b$ | $\eta$ (s) | N |
|---|---|---|---|---|
| 2.0 | 0.22 | 8.5 | 200 | 3 |

Figure 7 presents the successful fitting of this set of parameters on the creep response of four triaxial tests at four different confining pressures, for a given deviator "q" of 800 kPa. Figure 7a presents the results in terms of kinetics for the axial and the radial strain versus time. The results show that the set of parameters allows to fit correctly both the axial and radial strains curves. The comparison between the simulation and the experimental strains for the unconfined sample (curve in black) shows the difficulty of the model to simulate unconfined conditions. For the other curves, numerical and experimental results are very close. Figure 7b presents the results in terms of loading path, with the volumetric strain as function of the axial strain. Numerical and experimental results are similar, but computed volumetric strains (dashed lines) are always slightly lower than the experimental strains: the model overestimate dilatancy at given axial strain. On an overall analysis, the model gives realistic results, and the experimental ranking is respected by the simulations.

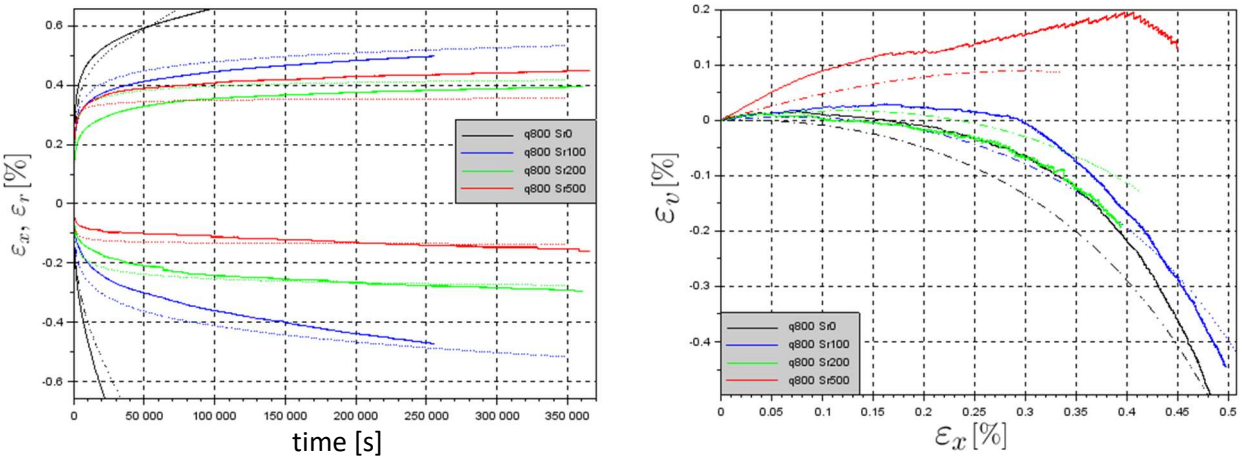


**(a)** Axial and radial strains. **(b)** Volumetric strain.

Figure 7. Experimental and numerical results of 4 triaxial tests at q=800 kPa.

## 8. RAILWAY STRUCTURE SIMULATIONS UNDER CREEP LOADING

Cast3m is an open-source numerical simulation software developed by the French CEA. It is based on the Finite Element Method to solve mechanical and thermal problems. The Perzyna flow rule was implemented in Cast3m as a user subroutine. Simulations were first performed on a single finite element to validate the implementation. Figure 8 shows an example of the comparison between theoretical (analytical) and numerical (Cast3m) responses to a given stress state.

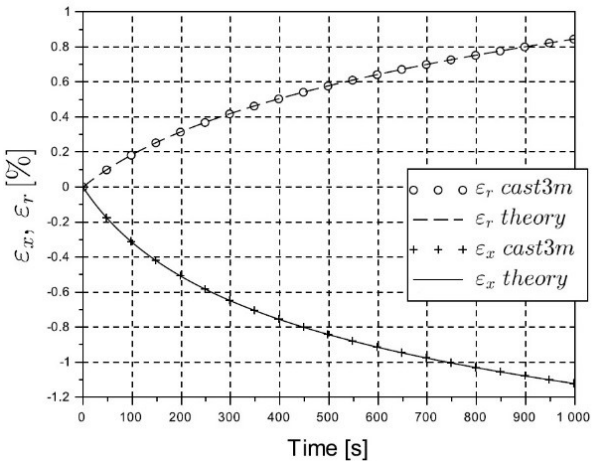


Figure 8. Validation of the numerical implementation on a single Gauss point (theoretical and Cast3m response).

One of the railway structures proposed in the REVES project is presented in Figure 9a. In order to run FEM simulations using the Perzyna law implemented as user subroutine in Cast3m, a numerical model of the ballastless railway structure was designed (Figure 9b), and a heavy static load (250 kN axle load) was applied on it, representing a freight train stopped on the track for 300 years.

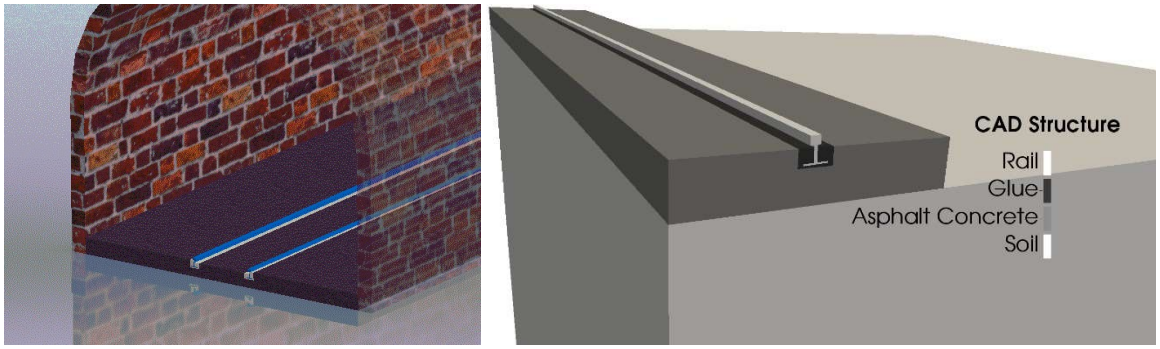


**(a)** **(b)**

Figure 9. (a) REVES Railway structure in a tunnel (concept) and (b) ¼ structure with soil and without the tunnel for further computations.

In order to optimize the computation time, only ¼ of the railway structure was modelled, using the two available symmetries. Due to this symmetry, a 62.5 kN load was distributed on the edge of the rail as shown in figure 10b, corresponding to a load of 250 kN per axle. The finite element mesh is presented on Figure 10a. Attention was given to the meshing density, to increase calculation accuracy close to the load, under the rail. The rail, the glue and the soil are assumed to have a linear elastic behaviour. Interfaces are perfectly bonded. The mechanical characteristics of the materials used in this simulation are presented in Table 4.

Table 4. Mechanical characteristics of the track components.

| Layer | Young modulus (MPa) | Poisson ratio |
|---|---|---|
| Rail | 200 000 | 0.28 |
| Glue | 2 | 0.49 |
| Asphalt Concrete | 400 | 0.35 |
| Soil | 120 | 0.35 |

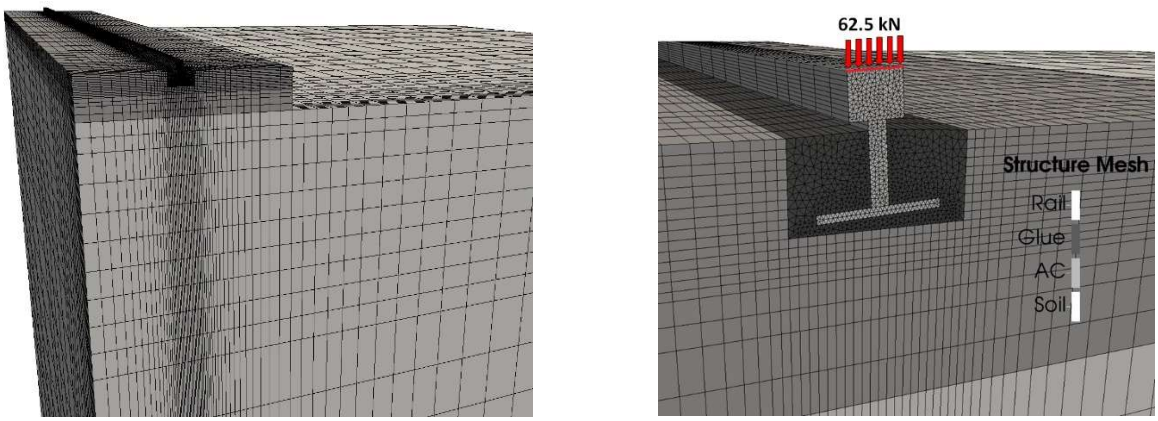


**(a)** **(b)**

Figure 10. (a) Meshing of the track section and (b) highlight of the mesh size on the rail and the load applied.

## 9. SIMULATION RESULTS

### 9.1. Displacements, strains and vertical settlement

Figure 11 depicts the results obtained from the FEM creep simulation. The deformed structure is shown in details in Figure 11a, amplified 50 times. It highlights the settlement of the soil under the asphalt concrete, under the center of the rail, as well as the deformation on the bottom of the groove in which the rails are inserted. Figure 11b shows the contour of the asphalt concrete layer before loading (initial state), at time step number one (just after loading) and at the final time step. The immediate response is considered as the elastic response, as the viscoplastic strains have not appeared yet. At this step, there is no really permanent settlement, distributed in the soil layer. The viscoplastic response at the final step leads to a more concentrate settlement under the groove, under the load and the rail.

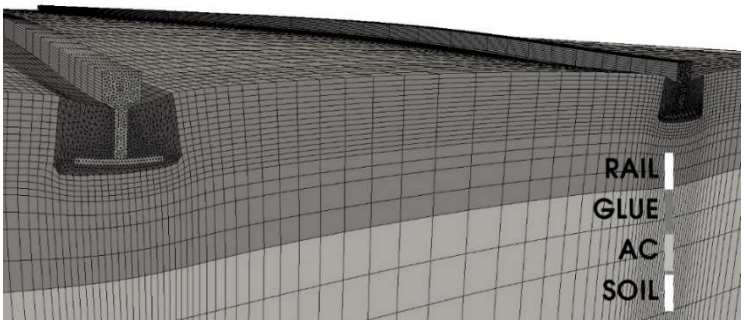


**(a)**

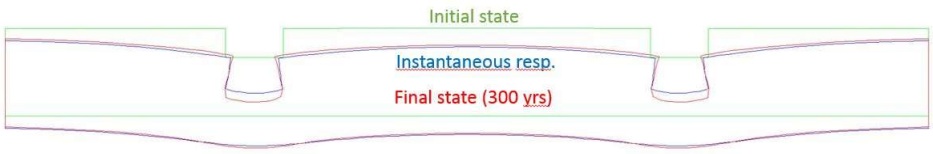


**(b)**

Figure 11. (a) Deformed structure at the end of the simulation (amplified 50 times) and (b) Evolution of the AC.

Figure 12 shows the vertical displacements of the rail after the first ten hours of simulation and after 30 years. The vertical displacement tends to stabilize, and reaches a final value of 1.39 mm, including both the elastic and the viscoplastic response. This result is acceptable according to the maximum specified displacement of 3.0 mm imposed by SNCF [2]. The viscoplastic behaviour leads to a rapid strain development at the beginning of the simulation, with 2/3 of the total settlement being reached after the first ten hours of test.

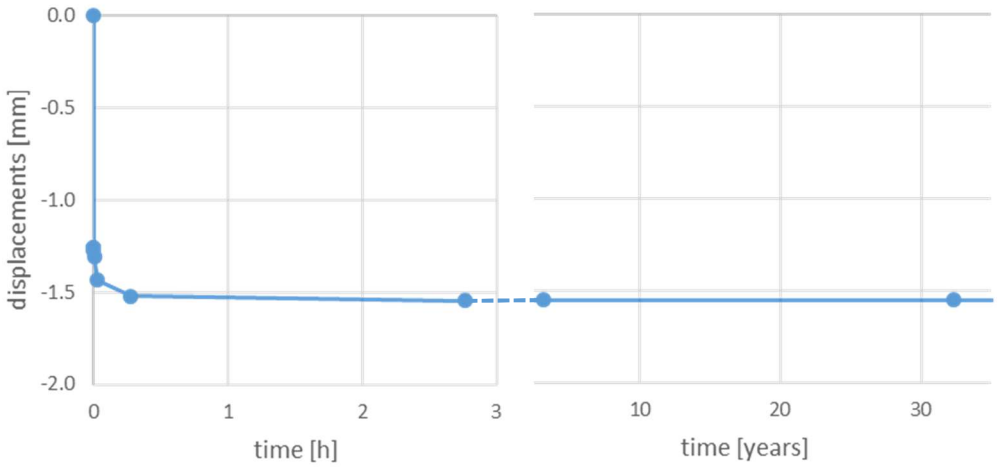


Figure 1. Evolution of vertical settlement on top-of-rail after (a) 3 hours and (b) 30 years of simulation.

### 9.2. Stress field in the vertical section under the load in the asphalt concrete

Figure 13 shows the evolution of the vertical and horizontal stress fields between the initial and the final time step in the asphalt concrete layer, under one rail. Figure 13a focuses on the vertical stress. An initial tensile stress (in red) is very low in the vertical direction, and tends to disappear completely over time. The compressive stress is initially strongly concentrated under the middle of the groove. It slightly spreads under the groove and the maximum local stress value decreases. The horizontal stress field is presented on Figure 13b. Tensile stress is represented in red and compressive stress in blue. At the initial step, the asphalt concrete layer under the groove behaves like a beam under flexion. Indeed, the bottom of the AC layer undergoes tensile stress while the bottom of the groove is submitted to compressive stress. The order of magnitude of the maximum tensile stress is 0.2 MPa. This represents a high level of tensile stress if maintained over time. However, at the final time step, the tensile stress at the bottom of the layer has completely dissipated, with the horizontal stress distributed in the layer, as usually observed for granular materials. It can be affirmed that the tensile stress vanishes thanks to the viscoplastic behaviour of the AC. The AC layer initially behaves like a beam under flexion and finally behaves more like an unbound material, highlighting the influence of both the bitumen and the granular skeleton. Figure 13c presents the shear stress fields (Von Mises stresses) at initial and final steps. It can be observed that the intensity of shear stress decreases between the initial and the final step. In the area under the groove, shear stress strongly decreases with time. At the final step, it remains relatively high, up to 0.5 MPa, at the interface of the groove and more particularly at the corners of the groove.

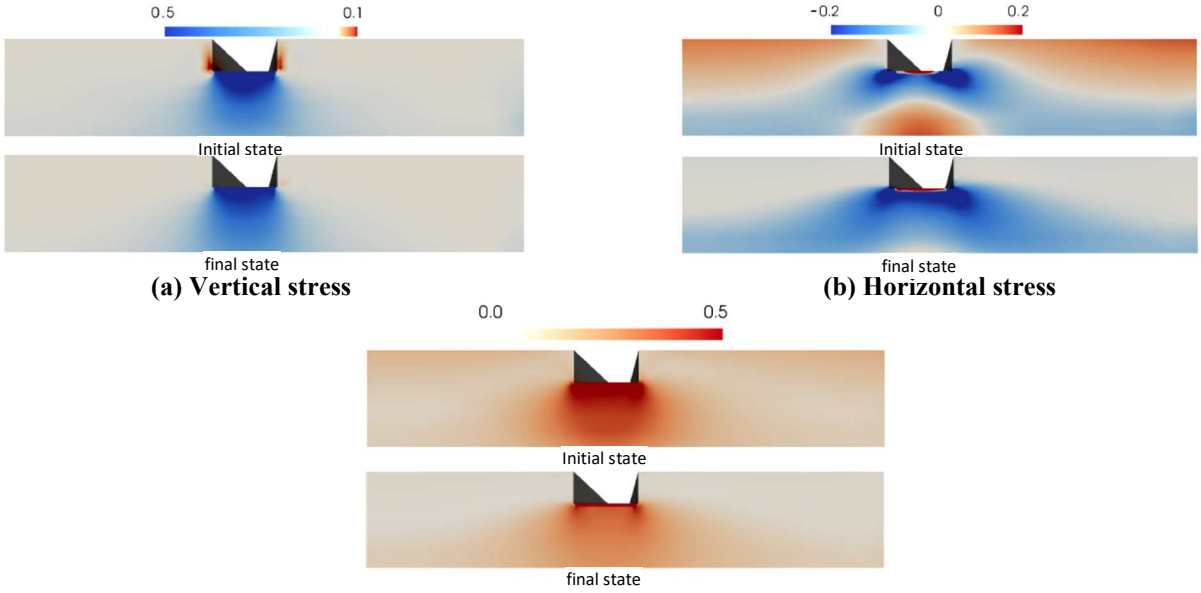


Figure 13. (a) Vertical stress, (b) horizontal stress and (c) shear stress inside the AC layer at initial and final times.

### 9.3. Evolution of stresses in the (p,q) plane

Figure 14 presents the initial (blue dots) and the final (green dots) stress states at every Gauss point of the vertical section of the GB4 below the load. The stresses are plotted in the (p,q) space. The initial yield surface of our VP model is also plotted on this figure.

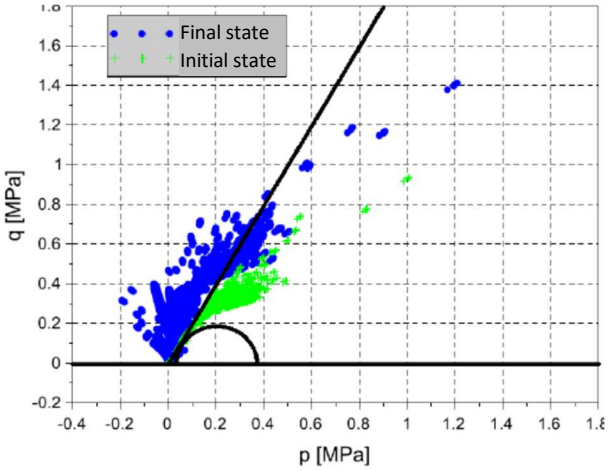


Figure 14. In the plan (p,q). Initial and final stress fields. Initial yield surface.

The initial stress state, in blue, varies between -0.2 MPa and 0.6 MPa for most of the points, but some of them reach a deviator of 1.4 MPa and a pressure of 1.2 MPa. Most of the points are located above the yield surface, implying viscoplastic flow. The negative values of "p" correspond to tensile stresses. Numerous points are initially under tensile stress, with shear levels reaching 0.4 MPa for some of them. At the end of the numerical simulation, all the points, in green, were located under the Drucker Prager curve. As the response stabilizes with time, it can also be assumed that at the end all the points are located under the circular caps, which evolved due to the hardening parameter of the VP model. Figure 14 shows the decrease of shear stress and the evanescence of tensile stress between the initial and the final state.

## 10. CONCLUSIONS

This paper summarizes some of the main results of a project aiming at designing innovative railway tracks by using AC as structural layer, without ballast nor sleepers. The analyses focuses on the viscoplastic behaviour of an asphalt concrete under heavy static loadings corresponding to a freight train standing on the track (the design of the structure to the fatigue damage due to the train traffic was also performed but not presented here).

The aim of this work is to assess the ability of such innovative structure to support static heavy loads. For that purpose, an experimental program was developed consisting in a standard characterization of an asphalt mixture of the GB4 type in terms of fatigue and stiffness (not presented here), and a series of triaxial creep tests at different deviator stress and confining combinations, mostly corresponding to the stress levels observed in simulations.
The main results are the following:

- The high performance of the GB4 and its resistance to heavy loads in terms of creep response and permanent strains were shown. The triaxial tests mostly featured the stabilization of creep tests when the material is confined.
- A standard viscoplastic model of Perzyna type was developed. The yield surface is a Ducker-Prager straight line closed by a circle used as a cap-model. A hardening rule was set up on this circle in order to allow the stabilisation of the strains under high confining pressures.
- A sequential and manual method allowed to identify the five parameters needed for the model. The model showed its ability to simulate the kinetics and the volumetric behaviour of the GB4 under different triaxial loading conditions.
- This model was implemented in the FEM code Cast3m as a user material.
- Several viscoplastic simulations were performed, aiming at predicting the creep behaviour of the railway track developed in the REVES project, under heavy loads. These simulations presented low settlements on top-of-rail, in accordance with the limits of SNCF standards.
- A strong decrease of tensile stress is observed in the asphalt concrete under creep loading. The AC layer initially behaves like a beam in flexion, and finally behaves more like an unbound material under vertical compression. These results look encouraging and tend to prove that such an innovative solution is reliable.

Several considerations need to be evaluated on further studies:

- From an experimental point of view, it seems necessary to optimize the triaxial testing program to identify the parameters for the proposed model. Indeed, in an ideal configuration, a minimum of five tests are needed to identify the parameters of the model. It currently represents five weeks of tests.
- We also need now to correlate our structural simulations to real structural experimentations in order to prove the reliability of the simulations. With this purpose, the presented railway structure was build inside IFSTTAR laboratory facilities, combined with a full scale loading system able to reproduce the static and dynamic loadings generated by a freight train on the track.
- Moreover, a track of 100 meters is going to be built in a private quarry. It will also be used to validate on the one hand this innovative railway infrastructure concept and also our numerical tool aiming at predicting creep and settlements.

## 11. ACKNOWLEDGEMENTS

The authors would like to thank SNCF-Réseau, the SNCF entity in charge of managing, operating and developing the French rail network, which founded the PhD thesis and the research presented in this paper. They would also like to thank all the partners of the French National project REVES.

## 12. REFERENCES

[1] IDRRIM (2019). Réalisation d'assise de voie ferrée en grave bitumen : Retour d'expérience de chantiers. Note d'information. https://www..idrrim.com/ressources/publications/30.04.2019_NOTE-D-INFORMATION-IDRRI.pdf

[2] Khairallah, D. et. Al, (2019). Monitoring of railway structures of the high speed line BPL with bituminous and granular sublayers. Construction and Building Materials, 211, 337-348.

[3] BACHMANN, H.; FREUDENSTEIN, S. Low-cost track systems RHEDA 2000 and GETRAC A3. European railway review, v. 10, n. 3, 2004.

[4] CARDONA, D. R.; DI BENEDETTO, H.; SAUZEAT, C.; CALON, N.; SAUSSINE, G. Use of bituminous mixture layer in high-speed line trackbeds. Construction and Building Materials, v. 125, p. 398-407. 2016.

[5] EN 12697-26 « méthodes d'essai pour mélange hydrocarboné à chaud : Module de rigidité ».

[6] EN, N. F. 12697-24 Spécification: Méthode d'essai pour mélange hydrocarboné à chaud: résistance à la fatigue. 2005.

[7] Sohm, J. Prédiction des déformations permanentes des matériaux bitumineux. Thèses de doctorat, Ecole Centrale de Nantes (ECN), March 2011.

[8] Sohm, J., Gabet, T., Hornych, P., Piau, J. M., & Di Benedetto, H. (2012). Creep tests on bituminous mixtures and modelling. Road Materials and Pavement Design, 13(4), 832-849.

[9] Lopez-Polanco, Octavio. Comportement d'un enrobé bitumineux sollicité par des rails posés sur des appuis continus. Thèses de doctorat, Ecole Centrale de Nantes (ECN), Septembre 2019.